Solution Structure of BSTI: A New Trypsin Inhibitor from Skin Secretions of *Bombina bombina*[†,‡]

K. Johan Rosengren, Norelle L. Daly, Martin J. Scanlon, and David J. Craik*

Institute for Molecular Bioscience, The University of Queensland, Brisbane, QLD 4072, Australia

Received November 14, 2000; Revised Manuscript Received January 18, 2001

ABSTRACT: The three-dimensional solution structure of BSTI, a trypsin inhibitor from the European frog *Bombina bombina*, has been solved using ^{1}H NMR spectroscopy. The 60 amino acid protein contains five disulfide bonds, which were unambiguously determined to be Cys (4−38), Cys (13−34), Cys (17−30), Cys (21−60), and Cys (40−54) by experimental restraints and subsequent structure calculations. The main elements of secondary structure are four β-strands, arranged as two small antiparallel β-sheets. The overall fold of BSTI is disk shaped and is characterized by the lack of a hydrophobic core. The presumed active site is located on a loop comprising residues 21−34, which is a relatively disordered region similar to that seen in many other protease inhibitors. However, the overall fold is different to other known protease inhibitors with the exception of a small family of inhibitors isolated from nematodes of the family *Ascaris* and recently also from the haemolymph of *Apis mellifera*. BSTI may thus be classified as a new member of this recently discovered family of protease inhibitors.

BSTI[1] is a 60 amino acid trypsin inhibitor isolated from the skin secretions of the European frog *Bombina bombina* (*1*). It is one of a number of peptides that have been discovered in amphibian skin (*2*−*4*), however, BSTI is about twice the size of most of the other peptides, which typically contain fewer than 30 amino acids. While the biological functions of all amphibian skin peptides have not yet been elucidated, the peptides can generally be classified as having regulatory or hormonal functions or antimicrobial activity. Many of the peptides in the first group are of great interest because of their similarities to mammalian hormones and neurotransmitters. Indeed, there are several cases where the characterization of an amphibian peptide has played a key role in the isolation of its mammalian analogue (*5*). The antimicrobial peptides, which are an important part of the amphibian innate immune system, are thought to have evolved to counter the microbe rich environment in which amphibians typically live (*6*, *7*). At least some of these peptides have the ability to disrupt microbial membrane functions, and the fact that in many cases they can adopt amphipathic helical structures suggests that oligomers of such helices form pores in the phospholipid bilayer (*8*−*10*).

The biological function of BSTI has not been unequivocally established, but it is has been suggested that it may be involved as a regulatory peptide in the processing reactions of other peptides in skin secretions (*1*). Many of these peptides are derived from larger precursor proteins that undergo a variety of processing reactions, including hydrolysis after Lys/Arg residues (*11*). In the skin secretions from *Xenopus spp* several enzymes involved in precursor processing have been characterized (*12*, *13*) and similar proteases are thought to occur in the *Bombina* genus. BSTI may control the activity of these proteases to prevent premature liberation or degradation of the skin peptides.

BSTI comprises 10 cysteine residues, which form five disulfide bonds, and is an inhibitor of trypsin and thrombin, with K_i values in the range 0.1−1 μM (*1*). Sequence homology searches suggest that the spacing of cysteine residues in BSTI is similar to that found in a family of protease inhibitors isolated from nematodes of the family *Ascaris.* A sequence comparison, which highlights the conservation of the 10 Cys residues of the peptides, is shown in Figure 1. This figure also illustrates the sequence homology between BSTI and a segment of the human von Willebrand factor, which has led to the interesting suggestion that this part of the von Willebrand factor may have a protease inhibitory effect (*1*). Recently, a new member of this proteinase inhibitor family was isolated from the hemolymph of *Apis mellifera*, the honeybee, (*14*) and the three-dimensional structure was determined using NMR spectroscopy (*15*). Previously, the 3D structures of two inhibitors from *Ascaris*, ATI and C/E-1, have been determined by NMR and X-ray crystallography respectively (*16*, *17*) and a model structure of BSTI has been proposed based on ATI (*1*).

In this report, we present the three-dimensional structure of BSTI determined by high resolution ^{1}H NMR. We show that it indeed has a similar fold to the family of inhibitors found in *Ascaris* and the *A. mellifera* peptide. Interestingly,

† This work was supported by a grant (D.J.C.) from the Australian Research Council.

‡ The coordinates for BSTI have been deposited in the PDB: ID code 1HX2.

* To whom correspondence should be addressed. Fax: 61-7-3365 2487. Phone: 61-7-3365 4945. E-mail: d.craik@imb.uq.edu.au.

[1] Abbreviations: BSTI, Bombina skin trypsin inhibitor; ATI, Ascaris trypsin inhibitor; NOE, nuclear Overhauser enhancement; DSS, 2,2-dimethyl-2-silapentane-5-sulfonate; TOCSY, total correlation spectroscopy; DQF−COSY, double quantum filtered correlation spectroscopy; NOESY, nuclear Overhauser enhancement spectroscopy; CSI, chemical shift index.

10.1021/bi002623v CCC: $20.00
Published on Web 03/17/2001

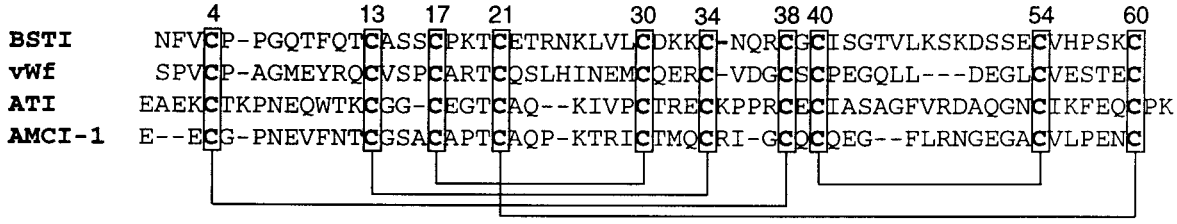

FIGURE 1: Sequence comparison of BSTI, a segment from human von Willebrand factor, residues 292−348, ATI (*16*) and a cathepsin G/chymotrypsin inhibitor from *A. mellifera* (*14*). The sequences are aligned to highlight the conservation of cysteine residues. The figure also shows the disulfide connectivity of the 10 cysteine residues.

the common fold of all of these peptides is different to other known serine protease inhibitors, apart from the conserved active-site region.

MATERIALS AND METHODS

Materials. BSTI was extracted and purified by Mignogna et al. (*1*). Samples prepared for NMR spectroscopy contained ~1.5 mM of the peptide dissolved in the following solvent systems: 90% H_2O/10% D_2O at pH 5.0 and 100% D_2O at pH 5.0. pH values were all measured at 298 K and no correction for deuterium isotope effects was made.

NMR Spectroscopy. Spectra were recorded on a Bruker DRX 750 spectrometer with sample temperatures of 293, 298, and 305 K. Spectra were also recorded on a Bruker ARX 500 with sample temperatures of 280 and 293 K. The carrier frequency was in all experiments set at the center of the spectra, on the water resonance frequency, and quadrature detection was used in both dimensions. All spectra were acquired in phase sensitive mode using TPPI (*18*). The following homonuclear spectra were recorded: double quantum filtered (DQF) COSY (*19*), TOCSY (*20*) with MLEV17 (*21*) isotropic mixing period of 80 ms, ECOSY (*22*) and NOESY (*23*) with mixing times of 75, 100, 150, 200, 250, and 300 ms. For the DQF−COSY experiment, the water proton signal was suppressed by lower power irradiation during the relaxation delay (1.8 s). Solvent suppression in TOCSY and NOESY experiments was achieved using a modified WATERGATE (*24*) sequence in which two gradient pulses of 1 ms duration and 6 G cm^{-1} strength were applied on either side of the binomial pulse. 2D spectra were collected over 4096 data points in the f_2-dimension and 512 increments in the f_1-dimension over a spectral width corresponding to 11 ppm. A series of 1D and TOCSY spectra were run immediately after dissolving the fully protonated sample in D_2O for identification of slowly exchanging amide protons.

All spectra were processed on a Silicon Graphics workstation using XwinNMR (Bruker). The f_1-dimension was generally zero-filled to 2048 real data points with the f_1- and f_2-dimensions being multiplied by a sine-squared function shifted by 90° prior to Fourier transformation. Chemical shifts were referenced to DSS. Spectra were analyzed within the program XEASY (*25*), and assignments of NOE cross-peaks were performed both manually and automatically using the automatic assignment program NOAH, which is a part of the DYANA (*26*) package.

Structure Calculations. Cross-peaks in NOESY spectra recorded in 90% H_2O/10% D_2O with a mixing time of 200 ms were integrated and calibrated and distance constraints were derived using DYANA. Corrections for pseudoatoms were added to distance constraints where needed (*27*). Backbone dihedral angle restraints were derived from $^3J_{HNH\alpha}$ coupling constants measured from line-shape analysis of antiphase cross-peak splitting in the DQF−COSY spectrum. Angles were restrained to $-120 \pm 40°$ for $^3J_{HNH_\alpha} > 9$ Hz and to $-60 \pm 30°$ for $^3J_{HNH_\alpha} < 5$ Hz. Additional ϕ angle restraints were applied where the intraresidue dαN(i,i) NOE was clearly weaker than the sequential dαN(i,i+1) NOE (*28*).

Stereospecific assignments of β-methylene protons and χ_1 dihedral angles were derived from $^3J_{\alpha\beta}$ coupling constants, measured from E.COSY spectra, in combination with NOE peak intensities (*29*). The χ_1 angles were restrained to $60 \pm 30°$, $180 \pm 30°$, or $-60 \pm 30°$. The quality of the data allowed restraints for 30 residues including 6 of the 10 cysteines. Positions of slowly exchanging amides were analyzed within the structures and in 12 cases hydrogen bonds were unambiguously assigned and added to the restraints. Structures were calculated using simulated annealing and energy minimization protocols within XPLOR version 3.851 (*30*). The starting structures were generated using random (ϕ, ψ) dihedral angles and energy minimized to produce structures with the correct local geometry. A set of 50 structures was generated by a torsion angle simulated annealing protocol (*31*, *32*), and structures consistent with restraints were subjected to energy minimization under the influence of the CHARMm force field (*33*, *34*).

RESULTS

BSTI was extracted from frog skin secretions as previously described (*1*). ^{1}H NMR spectra were recorded at 500 and 750 MHz at temperatures in the range 280−305 K. Assignments and structure calculations were made primarily based on spectra recorded at 293 K while spectra at other temperatures were used to resolve ambiguities. As the peptide was extracted from frog skin only unlabeled material was available. Therefore exclusively homonuclear spectra, including DQF−COSY, ECOSY, TOCSY, and NOESY were recorded. The spectral assignments were made using the well-established sequential assignment procedure (*35*) and are provided as supplementary information. Figure 2A shows the fingerprint region of the NOESY spectrum at 293 K with the sequential connectivities of the amino terminal half of the molecule labeled. The inset of panel 2B shows NOE connections to the hydroxyl proton of Thr44. In the course of the assignments, a peak at 5.68 ppm that displayed many NOEs to other protons, but could not be accounted for by either backbone HN, αH, or aromatic protons was observed. The peak was subsequently assigned to the slowly exchanging hydroxyl proton of Thr44. The fact that it was visible at all suggests that this Thr hydroxyl is well protected from

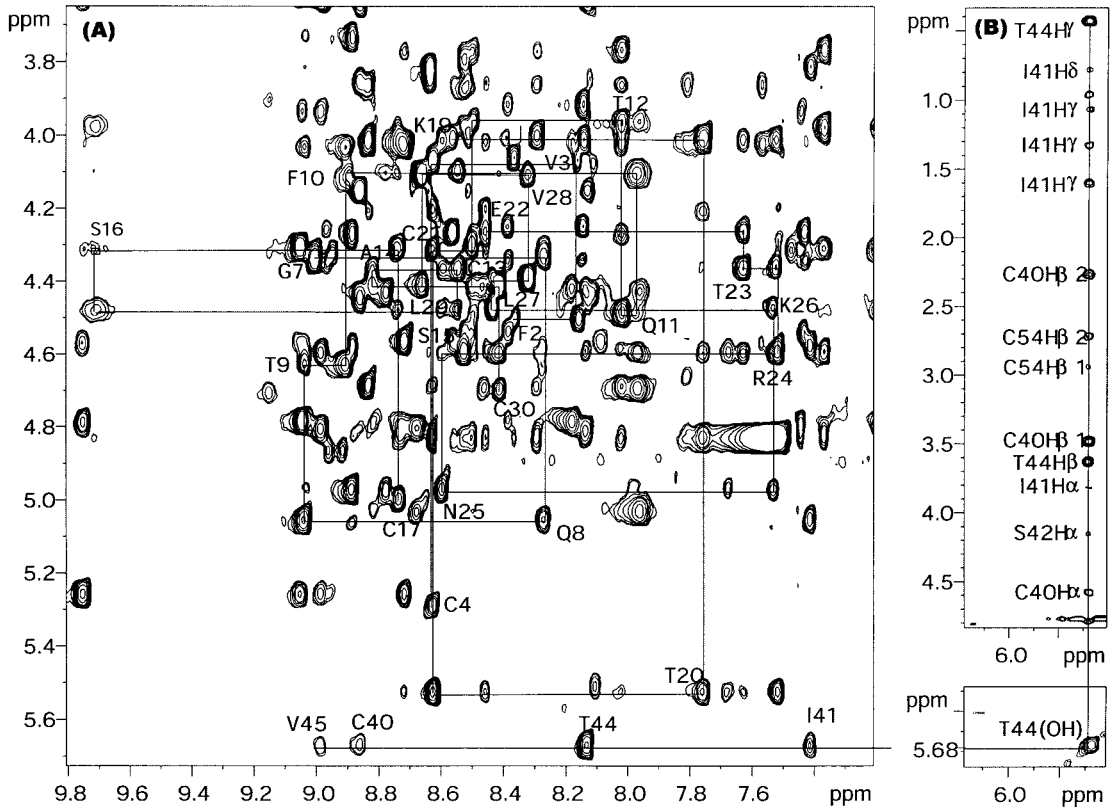

FIGURE 2: (A) Fingerprint region of the 200 ms NOESY spectrum (293 K, pH 5.0) of BSTI with resonances for the amino terminal part of the molecule labeled. The sequential walk is broken only by the proline residues 5, 6, and 18. (B) The inset highlights resonances involving the slowly exchanging hydroxyl of Thr44.

exchange with solvent and hence likely to be involved in a hydrogen bond. Subsequent structure calculations confirmed this to be the case.

BSTI contains four prolines (residues 5, 6, 18, and 57) all of which display strong $d_{\alpha i \rightarrow \delta i+1}$ NOEs in the D_2O NOESY spectrum. This confirms that the preceding amide bonds are all in the trans conformation.

Information on short and medium range NOEs, coupling constants, chemical shift index and slowly exchanging amide protons is shown in Figure 3. From these data, together with information about long-range NOEs, it is clear that the peptide contains no helical elements but has regions of extended β-type structure. The main elements of secondary structure are two β-sheets, each comprising two short antiparallel strands. The four β-strands involve residues 8−11, 37−40, 45−47, and 53−55, respectively. The arrangement of these strands together with identified NOEs and proposed hydrogen bonds, based on slowly exchanging amide protons, is presented in Figure 4.

Structure Determination. From the NOE data a set of 835 interresidual distance constraints, including 363 sequential, 177 medium-range, and 295 long-range restraints was derived. Further, slow exchange and coupling data allowed introduction of 24 restraints for 12 hydrogen bonds, 33 backbone dihedral angles, and 29 side-chain dihedral angles. Stereospecific assignments were possible for 15 pairs of β-methylene protons, including 6 of the 10 cysteine residues, three pairs of γ-methylene protons, three pairs of δ-methylene protons, two pairs of asparagine side-chain amide protons and two pairs of valine methyl groups. These restraints were used to calculate a set of 50 structures using a torsion angle simulated annealing protocol (*31*, *32*) within XPLOR (*30*). The resultant structures were energy minimized under the influence of the CHARMm force field (*33*, *34*).

From the final set of calculations a family of the 20 lowest energy structures was chosen to represent the solution conformation of BSTI, as shown in Figure 5. A summary of the statistics for this family is given in Table 1. The structures have only two distance violations greater than 0.2 Å and no dihedral violations greater than 2.0°. Further, they have good covalent geometry, which is indicated by small deviations from ideal bond lengths and bond angles. It is clear from both the superimposition of the structures (Figure 5) and the corresponding RMSD values (Figure 6) that the molecule has a precisely defined region, including elements of secondary structure, as well as a less defined loop region. Analysis of the structures with PROMOTIF (*36*) also identified several well-defined turns. The averaged pairwise RMSD values for the backbone atoms (N, C, Cα) over the entire molecule and for the well-defined regions (residues 4−13 and 36−60) are 0.80 and 0.58 Å respectively.

Disulfide Connectivity. No information about the disulfide connectivity of BSTI was available before this study was performed. Our assumption, based on the similarities in the pattern of cysteine residues, was that BSTI shared not only a trypsin inhibitory effect with ATI but also the same disulfide connectivity. This was supported by the experimental data, which included at least one NOE between each pair of cysteine residues corresponding to the disulfide bonds of ATI. A summary of the NOEs between cysteine residues is shown in Table 2. It is noteworthy that the types of NOEs observed are highly diagnostic of disulfide connectivity and

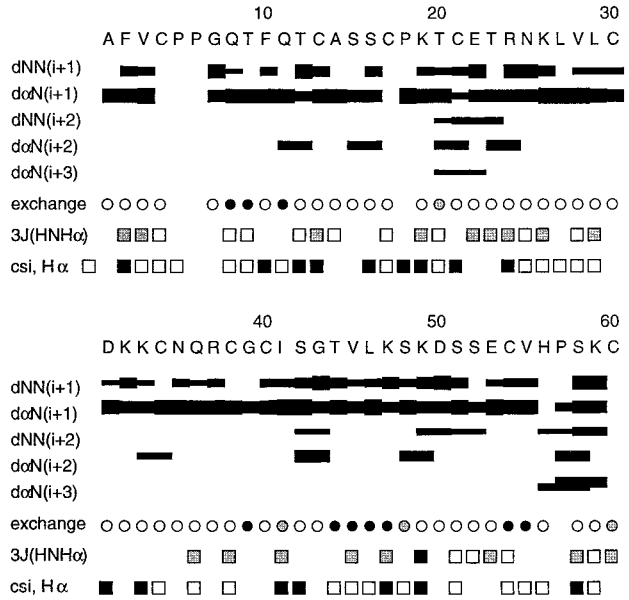

FIGURE 3: Summary of experimental NMR data on BSTI. Black bars represent NOEs present in the 200 ms NOESY spectrum (293 K, pH 5.0). The thickness of the bars corresponds to the NOE intensity. Empty circles represent amide protons in fast exchange with the solvent, filled represent amide protons still visible in experiments run 24 h after the sample was dissolved in D_2O and gray circles correspond to amides not fully exchanged after 6 h. Large and small $^3J_{NH-\alpha H}$ coupling constants are represented by empty and filled squares, respectively. Cases where a coupling constant could be measured but did not fall into any of these categories are indicated by a gray square. CSI values for Hα protons indicating potential helical and β-structure are represented by filled and empty squares, respectively.

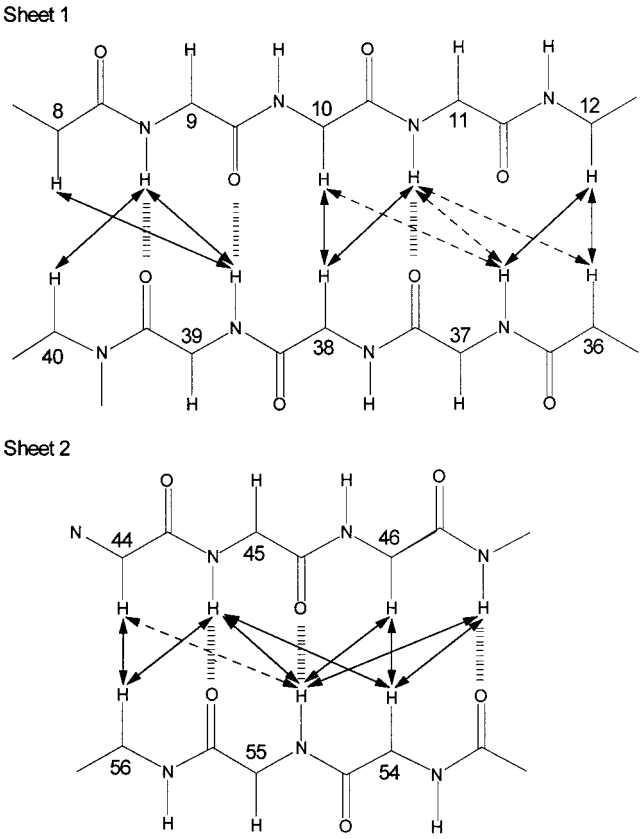

FIGURE 4: Schematic diagram of the two antiparallel β-sheets present in the BSTI structure. Arrows represent observed NOEs between protons in the sheets. Dashed arrows represent NOEs that could be present but that are not included in structure calculations due to overlap problems. Dashed lines correspond to hydrogen bonds proposed by MOLMOL (*29*) and subsequently introduced as restraints in structure calculations.

that there were no "antidiagnostic" NOEs (*37*) between Cys HN and Hα, which would indicate that the cysteines were not disulfide bonded. Furthermore, no NOEs were observed between cysteines that were not proposed to be coupled. These data were considered to be sufficient evidence for the introduction of the homology-based disulfide bonds in the initial stage of the structure calculations. The final converged structures clearly show that there is no other likely pairing of cysteines and that there is a large separation between different pairs of coupled cysteine residues in the three-dimensional structure.

Description of the Three-Dimensional Structure. As indicated by Figure 7, BSTI adopts a disk shaped structure. The disk has a diameter of approximately 24 Å in the view in Figure 7A and a width of 14 Å in the view in Figure 7B. The overall fold is very similar to that found in the family of protease inhibitors isolated from *Ascaris*, but it differs significantly from those seen in other serine protease inhibitors.

The superimposition of the final structures, shown in Figure 5, clearly illustrates the two different regions of the peptide. One region is well-defined and includes the two β-sheets, some well-defined turns and the carboxy terminal. The second region includes the N-terminus and the long, less defined, loop between residues 12 and 36 which includes the reactive site (residue 30−34). The poor definition of the amino terminal is most likely associated with flexibility of this region in solution, as is commonly observed in protein structures. The disulfide bond between Cys4 and Cys38, which is in the right-handed hook conformation in 15 out of 20 structures, serves as a link between the amino terminal and β-sheet 1. A turn is present between residues 5−8, which is defined as a type II β-turn in the majority of the structures. Residues 8−11 constitute β-strand A and this extended region is followed by a type VIII β-turn involving residues 11−14. The disulfide bonds between Cys13−Cys34 and Cys17−Cys30, which are the least well defined ones, flank the active site and possibly provide some stabilization for it. Their conformations correspond to a short right hook (10 of 20 structures) and a right-handed hook (13 of 20 structures), respectively. The disulfide bond between Cys21 and Cys60, which is exclusively in the left-handed spiral conformation in all 20 structures, ties the carboxy terminal to the loop comprising residues 12−36. Several ill-defined turns are present between residues 20−24 and 28−33. An inverse γ-turn, involving residues 35−37 precedes β-strand B, which includes residues 37−40. Another inverse γ-turn involving residues 41−43 is present between β-strand B and residues 45−47, which constitutes β-strand C. Finally, a type IV β-turn involving residues 48−51 forms the bridge between β-strand C and β-strand D, which includes residues 53−55. The last disulfide bond, Cys40−Cys54, is in a left-handed spiral conformation in all 20 structures and links the two β-sheets to each other. No hydrophobic core is present in the structure. Instead the disulfide bonds, which are widely spread in the structure, appear to have a major contribution to the stability of BSTI.

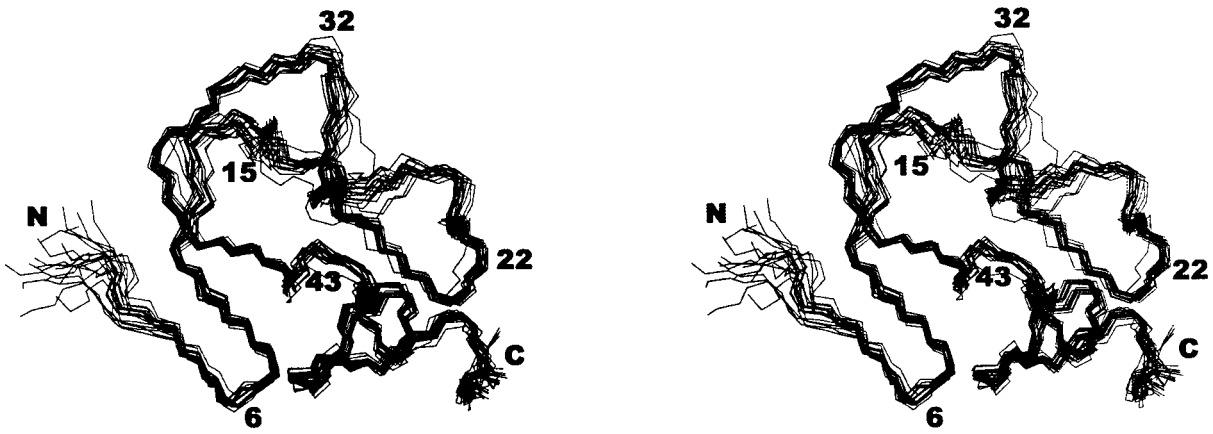

FIGURE 5: Stereoview of the backbone superimposition of the 20 final structures with lowest energy. N and C terminals and selected residues are labeled.

Table 1: Structural and Energetic Statistics for the Final Family of 20 BSTI Structures

mean RMS deviations from experimental restraints	
NOE (Å)	0.017 ± 0.0012
dihedral angles (deg)	0.16 ± 0.073
mean RMS deviations from idealized covalent geometry	
bonds (Å)	0.0078 ± 0.0003
angles (deg)	2.20 ± 0.037
impropers (deg)	0.17 ± 0.019
restraints violations	
NOE violations > 0.2 Å	2
maximum NOE violation (Å)	0.22
dihedral violations > 2°	0
maximum dihedral violation (deg)	1.88
mean energies (kJ mol^{-1})	
E_{noe}	7.90 ± 1.04
E_{cdih}	0.056 ± 0.034
E_{vdw}	−279.4 ± 4.4
$E_{bond} + E_{angle} + E_{improper}$	121.4 ± 5.0
E_{total}	−112.8 ± 3.8
pairwise RMSD	
backbone atoms 4−60 (N, Cα, C) (Å)	0.80 ± 0.21
heavy atoms (Å)	1.45 ± 0.23
backbone atoms (residues: 4−11, 37−60) (Å)	0.58 ± 0.18
heavy atoms (Å)	1.26 ± 0.20

Disordered regions of protein structures determined by NMR can result either from local flexibility or simply from a lack of sufficient NMR restraints. Disorder in the active-site region of BSTI is most likely due to flexibility, as further described in the discussion section. Poor definition among the family of structures is also seen for residues 15−17 and there is a significant broadening of the amide signal of Ser 16. This broadening may be caused by some flexibility in this region, or more likely by flexibility in the active site, which closely interacts with the region around residues 15−17. One other region of disorder is near residue 7, however, in this case the low S parameters appear to be due to a lack of experimental restraints. This conclusion is based on an analysis of interproton distances within the different structures and analysis of the spectra, which shows that overlap limits the measurement of a sufficient number of restraints to define the region around residue 7. Thus in this region the slight disorder in the structures is not likely to be due to local flexibility.

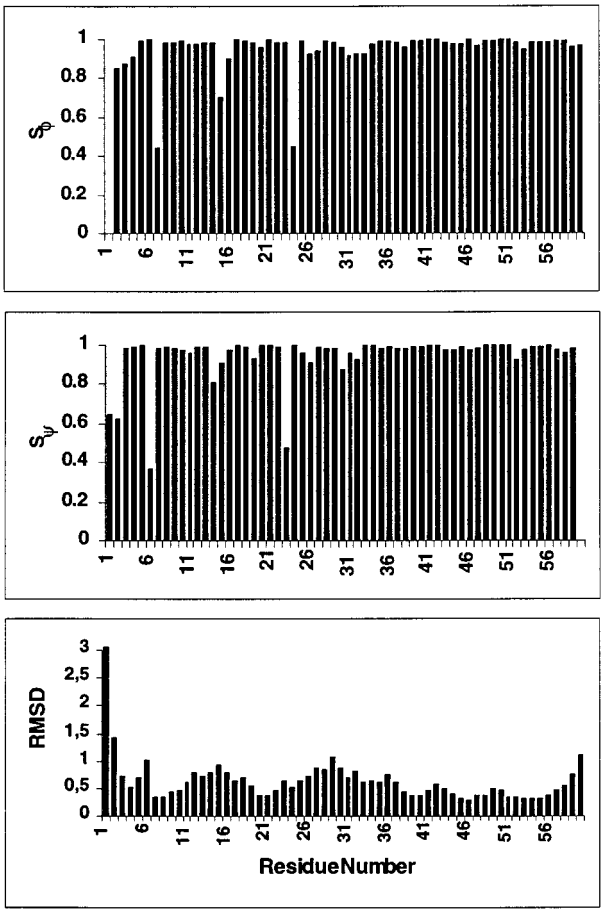

FIGURE 6: Angular order parameters (S values) for the backbone dihedral angles, ϕ (top) and ψ (middle) and RMSD of the backbone atoms of the averaged structure (bottom) versus the residue number.

Table 2: Summary of NOEs Observed between Coupled Cysteines

disulfide bond	Hα−Hα	Hα−Hβ	Hβ−Hβ	HN−Hβ	other NOEs
4−38		√	√		
13−34		√√	√√	√	
17−30		√			
21−60			√		
40−54		√	√√√		

DISCUSSION

Serine proteases play key roles in a number of different functions in the body, including peptide hormone release, blood coagulation, and complement fixation. They are also involved as pathogenic factors in different diseases, including some cancers and inflammatory processes (*38*, *39*). As a result of these functions, serine proteases and their inhibitors

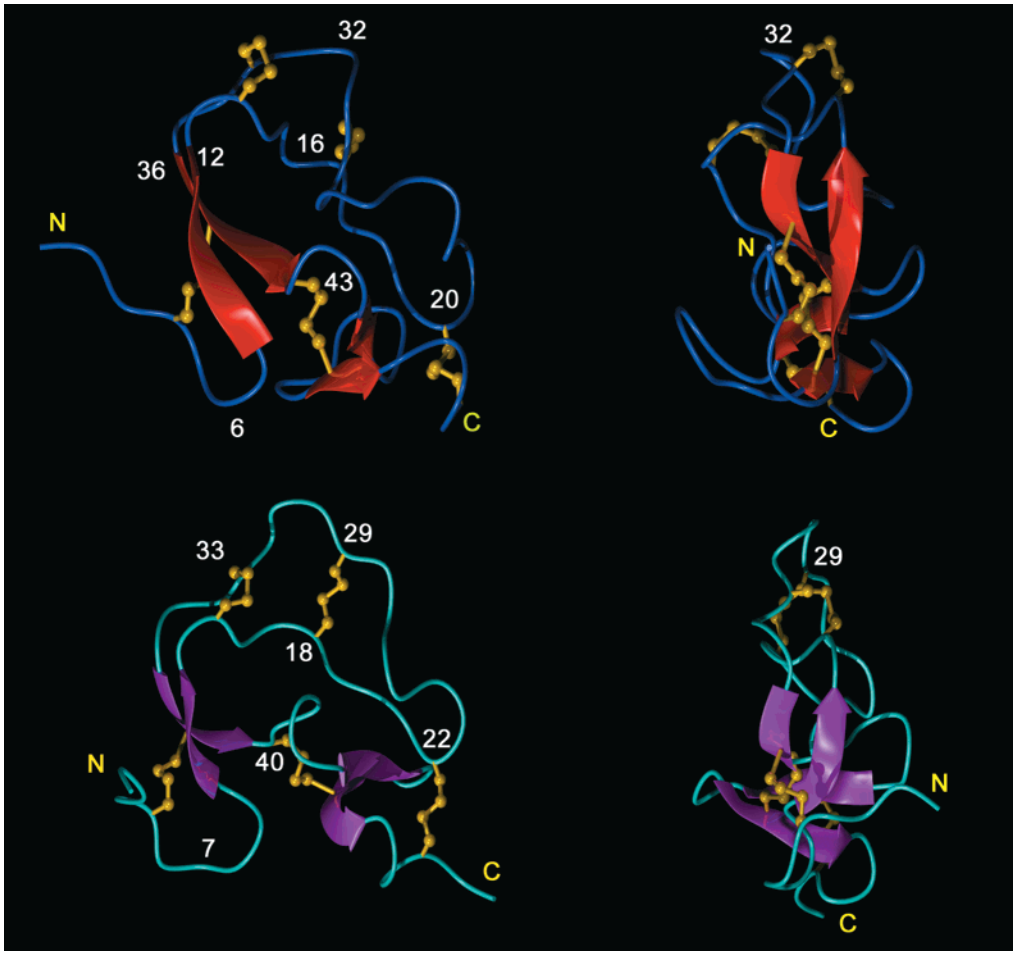

FIGURE 7: Comparison of the lowest energy structure of BSTI (view A and B, top of figure) and ATI (view C and D, bottom of figure). The β-sheets are presented as arrows in red and magenta. Disulfide bonds are shown in yellow in the ball-and-stick representation. N and C terminals and selected residues are labeled.

are interesting targets for drug design applications.

In this report, we have presented the three-dimensional solution structure of BSTI, a novel protease inhibitor isolated from the skin secretions of *B. bombina*. The suggestion, based on sequence homology, was that BSTI would adopt a fold similar to that found in the family of protease inhibitors from *Ascaris*. This was confirmed by our results which clearly show that BSTI and this family indeed have much, both locally and globally, in common. From Figure 7, it is clear that BSTI and ATI have the same flat "disc" shaped structure with the active site at the edge of the disk. Further, they have the same major elements of secondary structure—four β-strands arranged in two small, antiparallel β-sheets. When comparing the two structures it is clear that the most significant difference is the folding of the loop between cysteines 21 and 30 in BSTI. This can be explained by the fact that this loop in BSTI is two residues longer than the corresponding one in ATI. These two residues give rise to an extra turn in BSTI whereas ATI has a more extended conformation in this region.

No hydrophobic core is present in either of the structures. Instead, the fold is stabilized by the five disulfide bonds, the β-sheets, hydrogen bonds, and electrostatic interactions. In BSTI, 12 hydrogen bonds were identified based on information from exchange rates and preliminary structure calculations. Of these, six hold together the strands in the small β-sheet regions, one stabilizes the type II β-turn between residues 5−8, three stabilize the type IV β-turn between residues 41−44 and the other two are present between the amides of Cys60 and Leu46 and the carbonyls of His56 and Lys19, respectively.

In the absence of a core, the ATI structure contains two small regions of interacting hydrophobic residues at each side of β-sheet 2. Only one of these regions is partly conserved in BSTI and consists of residues Cys40, Ile41, Thr44, Val45, and Leu46. These interactions, together with the information about the hydrogen bonds, readily account for the unusually slow exchange rate of the Thr44 hydroxyl proton. The Ile41-Ser-Gly-Thr44 region forms a well-defined turn that is stabilized by three hydrogen bonds. The carbonyl of Ile41 acts as an acceptor to both the Thr44 amide proton and the Thr44 hydroxyl proton. Further, the Ile NH proton is also involved in a hydrogen bond. For this interaction the oxygen in the hydroxyl group of Thr44 acts as an acceptor. Around this network of hydrogen bonds is a hydrophobic pocket comprising the side chains of Thr44, Val45, and Ile41. The van der Waals surfaces of these groups almost completely bury the hydroxyl proton of Thr44. This effectively shields the hydroxyl proton from solvent and accounts for its visibility in the spectra. Normally, exposed hydroxyl groups exchange too rapidly to be observed in aqueous solutions.

The mechanism of inhibition of serine proteases is highly conserved among many of the small protein-based inhibitors.

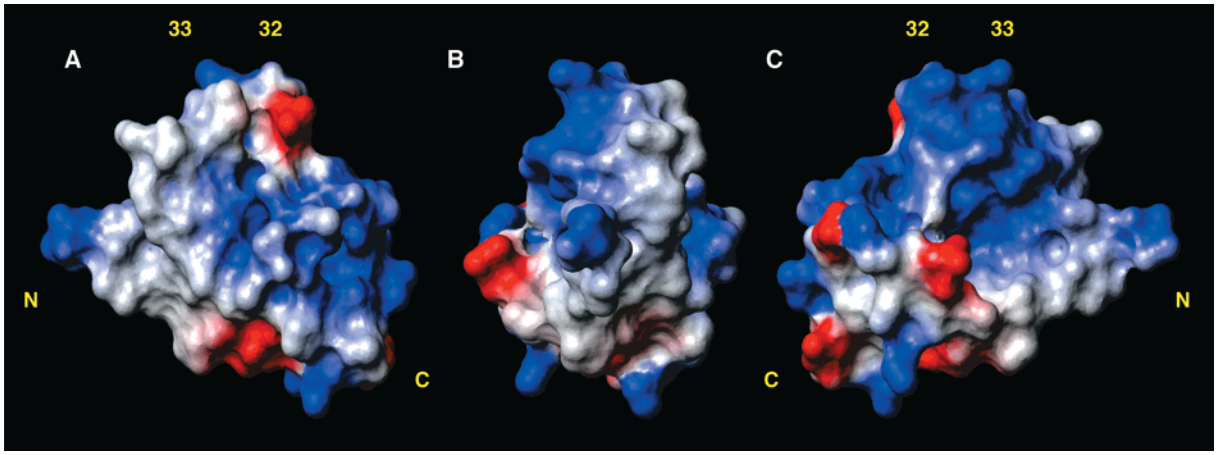

FIGURE 8: Three views of the BSTI surface electrostatic potential. Views B and C are rotated 90 and 180°, respectively, in relation to view A. Positively and negatively charged residues are colored blue and red, respectively. It is clear that the charged residues are mainly clustered on one face of the molecule. The amino and carboxy terminal as well as the charged lysine residues of the active site are labeled with residue numbers.

Table 3: Comparison of the Angles of the Peptide Backbone around the Scissile $P_1-P_{1'}$ Bond of BSTI and Some Other Protease Inhibitors

	P_3 (30)[a]		P_2 (31)		P_1 (32)		P_1' (33)		$P_{2'}$ (34)	
inhibitor	ϕ	ψ	ϕ	ψ	ϕ	ψ	ϕ	ψ	ϕ	ψ
BSTI, pH 5.0[a]	-162 ± 15	175 ± 30	-133 ± 25	-22 ± 11	-65 ± 11	-9 ± 21	-160 ± 12	157 ± 5	-117 ± 13	79 ± 3
ATI, pH 4.75[b]	−156	143	−85	−154	−74	40	−108	87	−122	121
ATI, pH 2.4[b]	−160	119	−68	−10	−63	−174	−117	−77	−170	114
1CCV[c]	−122	−41	−161	−178	−84	66	−172	153	−89	178
1CSE[d]	−139	168	−62	143	−115	45	−97	168	−117	110
2OVO[e]	−131	155	−87	173	−96	9	−58	139	−99	93

[a] Numbers correspond to residue numbers in the BSTI peptide, PDB code 1HX2. [b] The ATI data are from (*16*), PDB codes 1ATD and 1ATE. [c] 1CCV is a chymotrypsin inhibitor, AMCI-1 from honeybee (*15*). [d] 1CSE is eglin-c complexed with subtilisin Carlsberg (*42*). [e] 2OVO is ovomucoid third domain of silver pheasant (*43*).

The inhibitors often have the ability to bind to the enzyme in a substrate-like manner and form a tight substrate/enzyme complex. One peptide bond of the inhibitor is hydrolyzed but the product does not dissociate from the complex. The region interacting with the enzyme tends to be in an extended conformation on a surface exposed loop of the inhibitor. In BSTI, the reactive site is postulated to include residues 30−34 and is located in the long loop between the first and second β-strands, A and B. Figure 8 shows that this region of the molecule forms part of a face with a high local concentration of positive charge.

The local backbone angles of the reactive site region tend to be highly conserved in different serine protease inhibitors. Table 3 shows that the values for BSTI are generally similar to those of a range of other inhibitors, with the most significant differences being for residues 31 and 33, corresponding to the P_2 and $P_{1'}$ sites. However, any discussion of the significance of these specific differences must be made with caution, since Table 3 further shows that there is a significant degree of disorder among the backbone angles in the ensemble of NMR structures. The fact that this region is the most disordered in the molecule is not surprising. Residues in loops at the surface of proteins tend to be less defined than residues in the core. Further, NMR relaxation studies have been performed on other protease inhibitors and local motions have been detected around the active site (*40*). It appears that there is some flexibility in these regions that may be essential for enzyme binding. To further explore the reasons for any possible differences between BSTI and other serine protease inhibitors, a set of structure calculations, which included dihedral angle restraints that forced the structure to adopt the conserved angles, was performed. These arbitrary restraints did not induce any violations against the existing experimental data, suggesting that BSTI may indeed be similar in its active site region to the other inhibitors, but perhaps slightly more flexible, making it difficult to define its local backbone angles with high precision. This proposal of enhanced flexibility for BSTI is consistent with its substantially lower activity than other serine protease inhibitors: many have K_i values of 10^{-13} M but the value for BSTI is only 10^{-6} M.

It is interesting that the residues for which the average backbone angles for BSTI apparently differ most from other serine protease inhibitors are precisely those most affected by a pH-dependent conformational change seen in ATI (*16*). The biological function of ATI is to protect its organism, a nematode, from the digestive enzymes in the gut of the host. Studies were therefore performed to explore structural changes at the low pH at which ATI is active, and it was found that a drop in pH from 4.75 to 2.4 resulted in significant changes of the ψ angles for Thr30 and Glu32 (*16*). There are no biological reasons for performing similar studies on BSTI since it will not be exposed to such low pH conditions. However it is interesting to note that the unusual ψ angle seen for Thr30 in ATI at low pH (Table 3) matches very well with the unexpected value for the corresponding residue, Asp31 in BSTI. Further understanding of this phenomenon will await confirmation of the biological role of BSTI.

BSTI is likely to be involved as a regulatory peptide controlling the processing of other skin peptides. Many of these frog skin peptides are formed by hydrolysis of larger precursors and the processing reactions are often similar to that seen for mammalian counterparts (*41*). The first step of the peptides maturation process, which takes place before secretion, is generally cleavage of the pro-peptide after single or paired basic residues (*11*). Interestingly the skin peptides have been found to be further hydrolyzed by cleavage at Xaa−Lys bonds, where Xaa is Leu, Gly, Ala, or Lys, posterior to secretion (*9*). This modification serves most likely as an inactivation process to prevent toxic effects due to prolonged exposure. In *Xenopus laevis* several enzymes involved in processing reactions have been isolated (*12*, *13*). It is likely that similar enzymes are present in the *Bombina* genus and that BSTI controls the activity of these proteases. The active site of BSTI comprises the sequence Asp-Lys-Lys, which suggests that BSTI may have activity toward proteases similar to the one found in *X. laevis* and may be responsible for preventing prematuration or degradation of the skin peptides. However, no processing enzymes have so far been isolated from *B. bombina* and no structural or even sequence information is available for the proteases from *X. laevis*. Hence, it is too soon to speculate on possible interactions between BSTI and its receptor.

In summary, the three-dimensional structure of BSTI consists primarily of two antiparallel β-sheets and the structure is braced by five disulfide bonds whose connectivities could be unambiguously determined using the NMR data. It has a similar structure to a family of protease inhibitors previously only found in nematodes and in the honeybee. This family of inhibitors, with the exception of the active site, has no resemblance to any other known protease inhibitor. The active site is, however, similar to other serine protease inhibitors which suggests a similar mechanism of action.

ACKNOWLEDGMENT

D.J.C. is an Australian Research Council Professorial Fellow. M.J.S. is an ARC Postdoctoral Fellow. The Institute for Molecular Bioscience is a Special Research Centre of the Australian Research Council. We thank Prof. Günter Kreil for helpful comments and Giuseppina Mignogna, Dr. Donatella Barra, Christa Mollay, and Christa Tippelt for purifying the sample of BSTI.

REFERENCES

1. Mignogna, G., Pascarella, S., Wechselberger, C., Hinterleitner, C., Mollay, C., Amiconi, G., Barra, D., and Kreil, G. (1996) BSTI, a trypsin inhibitor from skin secretions of *Bombina bombina* related to protease inhibitors of nematodes. *Protein Sci. 5*, 357−362.
2. Bevins, C. L., and Zasloff, M. (1990) Peptides from frog skin. *Annu. Rev. Biochem. 59*, 395−414.
3. Anastasia, A., Erspamer, V., and Bucci, M. (1971) Isolation and structure of Bombesin and Alytesin, two analogous active peptides from the skin of the European amphibians. *Bombina Alytes*. *Experentia 27*, 166−167.
4. Lazarus, L. H., and Attila, M. (1993) The toad, ugly and venomous, wears yet a precious jewel in his skin. *Prog. Neurobiol. 41*, 473−507.
5. Erspamer, V., and Melchiorri, P. (1980) Active polypeptides: from amphibian skin to gastrointestinal tract and brain of mammals. *Trends Pharmacol. Sci. 1*, 391−395.
6. Barra, D., and Simmaco, M. (1995) Amphibian skin: a promising resource for antimicrobial peptides. *Trends Biotechnol. 13*, 205−209.
7. Charpentier, S., Amiche, M., Mester, J., Vouille, V., Le Caer, J.-P., Nicolas, P., and Delfour, A. (1998) Structure, synthesis and molecular cloning of Dermaseptins B, a family of skin peptide antibiotics. *J. Biol. Chem. 24*, 14690−14697.
8. Andreu, D., Aschauer, H., Kreil, G., and Merrifield, R. B. (1985) Solid-phase synthesis of PYLa and isolation of its natural counterpart, PGLa [PYLa−(4−24)] from skin secretion of *Xenopus laevis*. *Eur. J. Biochem. 149*, 531−535.
9. Giovannini, M. G., Poulter, L., Gibson, B. W., and Williams, D. H. (1987) Biosynthesis and degradation of peptides derived from *Xenopus laevis* prohormones. *Biochem. J. 243*, 113−120.
10. Westerhoff, H. V., Juretic, D., Hendler, R. W., and Zasloff, M. (1989) Magainins and the disruption of membrane-linked free-energy transduction. *Proc. Natl. Acad. Sci. U.S.A. 86*, 6597−6601.
11. Darby, N. J., and Smyth, D. G. (1990) Endopeptidases and prohormone processing. *Biosci. Rep. 7*, 907−917.
12. Darby, N. J., Lackey, D. B., and Smyth, D. G. (1991) Purification of a cysteine endo-peptidase which is secreted with bioactive peptides from the epidermal glands of *Xenopus laevis*. *Eur. J. Biochem. 195*, 65−70.
13. Kuks, P. M. F., Créminon, C., Leseney, A. M., Bourdais, J., Morel, A., and Cohen, P. (1989) *Xenopus laevis* skin Arg-Xaa-Val-Arg-Gly- endoprotease. *J. Biol. Chem. 264*, 14609−14612.
14. Bania, J., Stachowiak, D., and Polanowski, A. (1999) Primary structure of the cathepsin G/chymotrypsin inhibitor from the larval hemolymph of *Apis mellifera*. *Eur. J. Biochem. 262*, 680−687.
15. Cierpicki, T., Bania, J., and Otlewski J. (2000) NMR solution structure of *Apis mellifera* chymotrypsin/cathepsin G inhibitor-1 (AMCI-1): Structural similarity with Ascaris protease inhibitors. *Protein Sci. 9*, 976−984.
16. Grasberger, B. L., Clore, G. M., and Gronenborn, A. M. (1994) High-resolution structure of Ascaris trypsin inhibitor in solution: Direct evidence for pH-induced conformational transition in the reactive site. *Structure 2*, 669−678.
17. Huang, K., Strydnaka, N. C., Bernard, V. D., Peanasky, R. J., and James, M. N. (1994) The molecular structure of the complex of Ascaris chymotrypsin/elastase inhibitor with porcine elastase. *Structure 2*, 679−689.
18. Marion, D., and Wüthrich, K. (1983) Application of phase sensitive two-dimensional correlated spectroscopy (COSY) for measurements of ^{1}H-^{1}H spin−spin couplings in proteins. *Biochem. Biophys. Res. Comm. 113*, 967−974.
19. Rance, M., Sørensen, O. W., Bodenhausen, G., Wagner, G., Ernst, R. R., and Wüthrich, K. (1983) Improved spectral resolution in COSY ^{1}H NMR spectra of proteins via double quantum filtering. *Biochem. Biophys. Res. Commun. 117*, 479−495.
20. Braunschweiler, L., and Ernst, R. R. (1983) Coherence transfer by isotropic mixing: application to proton correlated spectroscopy. *J. Magn. Reson. 53*, 521−528.
21. Bax, A., and Davis, G. D. (1985) MLEV-17 based two-dimensional homonuclear magnetization transfer spectroscopy. *J. Magn. Reson. 65*, 355−360.
22. Greisinger, C., Sørenson, O. W., and Ernst, R. R. (1987) Practical aspects of the E. COSY technique: measurement of scalar spin−spin coupling constants in peptides. *J. Magn. Reson. 88*, 177−185.
23. Jeener, J., Meier, B. H., Bachmann, P., and Ernst, R. R. (1979) Investigation of exchange processes by two-dimensional spectroscopy. *J. Chem. Phys. 71*, 4546−4553.
24. Piotto, M., Saudek, V., and Sklenar, V. (1992) Gradient-tailored excitation for single-quantum NMR spectroscopy of aqueous solutions. *J. Biomol. NMR 2*, 661−665.
25. Eccles, C., Güntert, P., Billeter, M., and Wüthrich, K. (1991) Efficient analysis of protein 2D NMR spectra using the software package EASY. *J. Biol. NMR 1*, 111−130.

26. Güntert, P., Mumenthaler, C., and Wüthrich, K. (1997) Torsion angle dynamics for NMR structure calculation with the new program DYANA. *J. Mol. Biol. 273*, 283−298.
27. Wüthrich, K., Billeter, M., and Braun, W. (1983) Pseudo-structures for the 20 common amino acids for use in studies of protein conformations by measurement of intermolecular proton−proton distance restraints with nuclear magnetic resonance. *J. Mol. Biol. 169*, 949−961.
28. Clubb, R. T., Ferguson, S. B., Walsh, C. T., and Wagner, G. (1994) Three-dimensional solution structure of *Escherichia coli* periplasmic cyclophilin. *Biochemistry 33*, 2761−2772.
29. Koradi, R., Billeter, M., and Wüthrich, K. (1996) MOLMOL: a program for display and analysis of macromolecular structures. *J. Mol. Graphics 14*, 51−55.
30. Brünger, A. T. (1992) *X-PLOR Manual Version 3.1*, Yale University, New Haven, CT.
31. Rice, L. M., and Brünger, A. T. (1994) Torsion angle dynamics: reduced variable conformational sampling enhances crystallographic structure refinement. *Proteins 19*, 277−290.
32. Stein, E. G., Rice, L. M., and Brünger, A. T. (1997) Torsion-angle molecular dynamics as a new efficient tool for NMR structure calculation. *J. Magn. Reson. 124*, 154−164.
33. Clore, G. M., Nilges, M., Sukuraman, D. K., Brünger, A. T., Karplus, M., and Gronenborn, A. M. (1986) The three-dimensional structure of α1-purothionin in solution: combined use of nuclear magnetic resonance, distance geometry and restrained molecular dynamics. *EMBO J. 5*, 2729−2735.
34. Brooks, R. R., Bruccoleri, R. E., Olafson, B. D., States, D. J., Swaminathan, S., and Karpulus, M. (1983) CHARMm: A program for molecular energy minimisation and dynamics calculations. *J. Comput. Chem. 4*, 187−217.
35. Wüthrich, K., (1986) *NMR of proteins and nucleic acid*, John Wiley and Sons Inc., New York.
36. Hutchinson, E. G., and Thornton, J. M. (1996) PROMOTIF: a program to identify and analyse structural motifs in proteins. *Protein Sci. 5*, 212−220.
37. Klaus, W., Broger, C., Gerber, P., and Senn, H. (1993) Determination of the disulphide bonding pattern in proteins by local and global analysis of nuclear magnetic resonance data. application to flavoridin. *J. Mol. Biol. 232*, 897−906.
38. Hörl. H., and Heidland. A. (1982) Proteinases: Potential role in health and disease. *Advances in Experimental Medicine and Biology*, Vol. 167, Plenum Press, New York.
39. Schnebli, H. P., and Braun, N. J. (1986). Proteinase inhibitors as drugs. In *Proteinase inhibitors* (Barett, A. J., and Salvesen, A., Eds.) pp 613−627, Elsevier, The Netherlands.
40. Peng, J. W., and Wagner, G. (1992) Mapping of the spectral densities of N−H bond motions in eglin c using heteronuclear relaxation experiments. *Biochemistry 31* (36), 8571−8586.
41. Gibson, B. W., Poulter, L., Williams, D. H., and Maggio, J. E. (1986) Novel peptide-fragments originating from PGLA and the cerulein and xenopsin precursors from *Xenopus laevis*. *J. Biol. Chem. 261*, 5341−5349.
42. Bode, W., Epp, O., Hubert, R., Laskowski, M., and Ardelt, W. (1985) The crystal and molecular structure of the third domain of silver pheasant ovomucoid (OMSVP3). *Eur. J. Biochem. 147*, 387−395.
43. Bode, W., Papamokos, E., and Musil, D. (1987) The high-resolution X-ray crystal structure of the complex formed between subtisilin Carlsberg and eglin c, an elastase inhibitor from the leech *Hirudo medicinalis*. *Eur. J. Biochem. 166*, 673−692.

BI002623V